Moisture Independent Measurement of Solid Concentration in Gas-Solid Flows Using Dual-Frequency Dipole Antennas

Dayang Wang, Danian Zhang, Yutao Wang, Lijuan Wang, *Senior Member*, *IEEE*, and Yong Yan, *Fellow*, *IEEE*

***Abstract*—In gas-solid two-phase flow, the accuracy of solid concentration measurement is significantly affected by the unknown and varying moisture content in the solid phase, particularly when the used method is sensitive to the moisture content. To address this issue, a new method that uses a novel microwave transmission sensor working at two frequencies and a novel decoupling method is proposed to achieve moisture independent solid concentration measurement. A dual-frequency resonant printed dipole antenna is designed using finite element simulation method, and the microwave transmission sensor which can work at two frequencies is formed by two dipole antennas. A simple and effective decoupling method is proposed to extract moisture content from dual-frequency phase shift information, enabling solid concentration measurement. The flow structures of roping flow with varying solid concentrations and moisture contents are used to verify the proposed method. Experimental results demonstrate that the dual-frequency phase shifts of the microwave transmission sensor are both sensitive to the solid concentration and moisture content. Therefore, only relying on the phase shift information from a single frequency cannot accurately measure solid concentration under conditions of varying moisture content. The decoupling method proposed in this study, based on dual-frequency phase shift information, can accurately determines moisture content. Consequently, it enables solid concentration measurement in gas-solid flows with relative errors within ±5% under conditions of varying moisture content.**

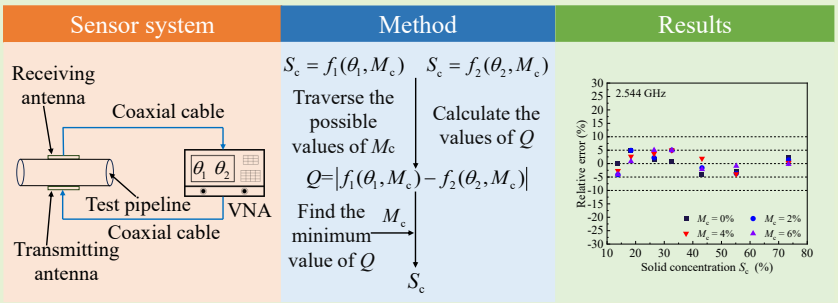

***Index Terms*—dual-frequency microwave dipole antenna, gas-solid two-phase flow, moisture content, solid concentration measurement**

I. Introduction

Gas-solid two-phase flow is commonly encountered in industrial processes such as the pneumatic conveying of coal powder in blast furnaces. Accurate measurement of solid concentration is essential for the effective control and management of the pneumatic conveying process. By precisely monitoring solid concentration, adjustments can be made to the air and material flow to prevent issues such as pipeline clogging, excessive wear on equipment, or energy inefficiencies, ultimately improving system reliability and operational efficiency. However, in contrast to measuring single-phase fluids, the coexistence and non-uniform distribution of solid phase and gas phase in gas-solid two-phase flow introduce difficulty in achieving accurate measurements of solid concentration. Furthermore, the unknown moisture content within the solid phase brings an additional challenge to the accurate measurement of solid concentration.

Current methods for measuring parameters in gas-solid two-phase flow include electrostatic method [1]-[3], capacitive method [4]-[6], ultrasonic method [7]-[9], radiation method [10] [11], and microwave method [12]-[15]. The electrostatic method is based on the electrostatic properties of solids and is highly sensitive. However, its measurement results are influenced by particle characteristics and moisture content. The capacitive method relies on dielectric properties for measurement, offering low cost and non-contact measurement. However, the non-uniform distribution of solids and moisture content affect the accuracy of solid concentration measurements. The ultrasonic method provides a fast response and is cost-effective, but the non-uniform solid distribution and variations in solid acoustic properties also present challenges

This work was supported by the National Natural Science Foundation of China under Grant 62303097, Grant 62473092. *(Corresponding author: Yutao Wang.)*

Dayang Wang is with the College of Information Science and Engineering, Northeastern University, Shenyang 110819, China, and also with the School of Engineering, Mathematics and Physics, University of Kent, Canterbury, CT2 7NT, U.K. (e-mail: wangdayang@ise.neu.edu.cn)

Danian Zhang and Yutao Wang are with the College of Information Science and Engineering, Northeastern University, Shenyang 110819, China. (e-mail: 2270842@stu.neu.edu.cn; wangyutao@ise.neu.edu.cn).

Lijuan Wang is with the School of Engineering, Mathematics and Physics, University of Kent, Canterbury, CT2 7NT, U.K. (e-mail: l.wang@kent.ac.uk).

Yong Yan is with Hangzhou International Innovation Institute, Beihang University, Hangzhou 311115, China. (e-mail: yongyan@buaa.edu.cn).

for ultrasonic measurements. The radiation method can achieve accurate solid concentration measurements, but it comes with drawbacks such as safety risks, high costs, and regulatory restrictions. With its advantages of non-contact measurement, fast response, high sensitivity, and multiple sensing effects, the microwave method shows promising application prospects in multiphase flow measurement. Particularly, it has been extensively researched and applied in multiphase flows involving water phase. As the dielectric property of water is distinctive from other phases in multiphase flows, microwave transmission and resonance method [16]-[23] are investigated to measure the water holdup. In comparison with multiphase flows involving a water phase, the application of microwave methods in gas-solid two-phase flow measurement has received limited attention. Guo and Zhang [12] designed a concentration gauge composed of an emission antenna and a receiving antenna and utilized the attenuation of microwave signals passing through coal powder to calculate the solid concentration. Pang et al. [13] developed a non-intrusive mass flow measurement system with a fixed working frequency and utilized the correlation between received microwave signal power and solid concentration to estimate the particle concentration. Akhter et al. [14] employed a circular waveguide with a resonant iris structure to assess solid concentration in the gas stream. This was achieved through an analysis of the scattering coefficients of the transmitting and receiving probes. Zou et al. [15] used a 16-antenna microwave tomography sensor to capture electrical signals between antenna pairs, subsequently using image reconstruction algorithms to generate spatial images and thereby infer solid concentration.

The aforementioned studies on gas-solid two-phase flow measurement were conducted under the assumption of a constant permittivity for the solid. However, in some industrial processes, the situation that moisture in the solid changes is often encountered. The varying and unknown moisture brings new challenges to the solid concentration measurement using microwave method. Currently, methods for measuring solid concentration with varying moisture in gas-solid two-phase flow have not been fully developed. Only a limited number of studies have utilized the microwave method to measure solid concentrations with varying moisture. Penirschke et al. [24] combined two different microwave sensors to achieve moisture insensitive solid concentration measurement. The combined sensor required more installation space and the integration of the sensor system was complex. Additionally, the sensor system was sensitive to the cross-sectional flow distribution. Wang et al. [25] proposed a combined sensor system including a microwave sensor and a capacitive sensor to measure solid concentration without being influenced by moisture. The performance of the combined sensor system was affected by the nonuniform sensitivity distribution and low sensitivity of the capacitive sensor. Wang et al. [26] developed a microwave resonant cavity sensor to measure solid concentration with varying moisture. This method required prior knowledge of the sensor outputs when the pipe was full of air and full of solid.

In this study, a new method that uses a novel microwave transmission sensor working at two frequencies and a novel decoupling method is proposed to achieve moisture independent solid concentration measurement. The sensor is formed by two dual-frequency resonant printed dipole antennas which are designed using finite element simulation method. The sensor simultaneously senses the changes in both solid concentration and moisture content based on the phase shifts at two working frequencies. Afterward, the decoupling method is proposed to simultaneously obtain moisture content and solid concentration from dual-frequency phase shift information. Experiments were carried out and the experimental results demonstrate that this method can achieve moisture independent solid concentration measurements in gas-solid two-phase flow. Compared to the existing works mentioned above, the proposed method utilizes only one compact microwave transmission sensor that operates at two frequencies. The phase shifts at both frequencies are sensitive to solid concentration and moisture but not sensitive to the solid distribution. By proposing the decoupling method, moisture independent solid concentration measurement is achieved without requiring prior knowledge of sensor outputs when the pipe is full of air and full of solid. This study provides a new approach for accurately measuring solid concentration under varying moisture conditions.

II. Measurement Methodology and System Design

A. Measurement methodology

The microwave transmission method measures the gas-solid flows based on the amplitude attenuation and phase shift effects of the microwaves caused by the medium. When fixed-frequency microwaves are emitted from the transmitting antenna of a sensor, propagate through medium, and are received by the receiving antenna, the amplitude attenuation A_1 (dB) and phase shift θ_1 (degree) are both related to the complex relative permittivity of the medium [27]. For gas-solid flows with varying moisture, the complex relative permittivity is dependent on the solid concentration S_c and moisture content M_c. Therefore, the amplitude attenuation A_1 and phase shift θ_1 are both related the solid concentration S_c and moisture content M_c. Their relationships can be established as

$$S_c = F_1(A_1, M_c) \tag{1}$$

$$S_c = f_1(\theta_1, M_c) \tag{2}$$

From equation (1) and (2) we can see that depending only on the measured A_1 or θ_1 values to measure solid concentration will be affected by unknown moisture content M_c. Compared to amplitude attenuation, microwave phase shift exhibits higher sensitivity and is more suitable for measuring phase holdups and solid concentration in multiphase flow [25][27][28]. Therefore, microwave phase shift was selected for the measurements in this study. However, when measuring solid concentration in gas-solid flows using phase shift at a single frequency, the measurement is affected by the unknown moisture content, as shown in equation (2). If the sensor can work at another frequency and the phase shift θ_2 at this working frequency also has relationship with solid concentration S_c and moisture content M_c, and the relationship can be established as

$$S_c = f_2(\theta_2, M_c) \tag{3}$$

The combined use of equation (2) and (3) makes it possible to simultaneously determine the moisture content and solid concentration. To determine the M_c and S_c, a decoupling method is proposed and a new parameter Q which is the absolute value of the difference between the S_c measured using two frequencies is defined as

$$Q=\left|f_1(\theta_1, M_c) - f_2(\theta_2, M_c)\right| \tag{4}$$

Since the sensor measure the same gas-solid flows using two working frequencies, the measured S_c should be the same when the M_c is determined. Therefore, when the M_c is accurately determined, Q will take the minimum value. By traversing possible values M_c, the values of Q with different M_c are calculated. Then, find the minimum value of Q, the corresponding M_c is the true moisture content. When the M_c is determined, the solid concentration S_c can be determined using equation (2) or (3). In this study, to achieve dual-frequency measurement, a novel microwave sensor system using dual-frequency dipole antennas is designed. Based on the two phase shifts obtained from experiments, a decoupling method is developed to extract the moisture content M_c. Furthermore, the two phase shifts are respectively used to predict the solid concentration S_c. The flowchart of the proposed method is shown in Fig. 1.

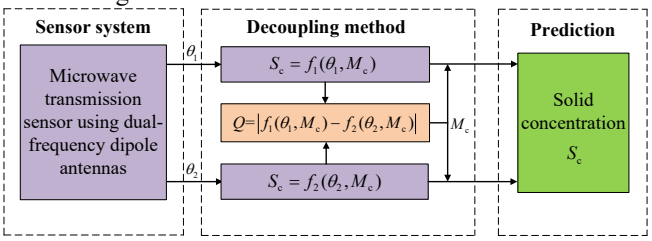

Fig. 1. Overall flowchart of the proposed methods.

B. Design of dual-frequency printed dipole antenna

When using a dual-frequency method for solid concentration measurement, the design of suitable transmitting and receiving antenna to form a sensor is crucial. A dipole antenna has two resonant frequencies by designing its structures [29]. It can have a broad operating frequency range, offering flexibility in designing working frequencies. It features a simple structure and easy impedance matching [30]. These advantages make it suitable for use as both transmitting and receiving antennas to form a novel dual-frequency sensor, achieving dual-frequency measurement of solid concentration.

In this study, a new dual-frequency printed dipole antenna is designed using finite element simulation method, and its configuration is shown in Fig. 2. The antenna consists of a dielectric plate, two high-frequency dipole arms, two low-frequency dipole arms, a microstrip balun, a microstrip transmission line, and an antenna feed surface. The dielectric plate, with a length of 90 mm and a width of 80 mm, is made of FR4 epoxy resin with a dielectric constant ε_r of 4.4, and a thickness of 1.6 mm [31], while the other elements are conductors. The width of the microstrip transmission line is 2 mm, and to achieve 50 Ω impedance matching, a microstrip balun is employed as an impedance matching device [32]. The excitation signal is fed into the antenna through the feed surface, passing through the microstrip balun and the transmission line before reaching the dipole arms. Within the microstrip transmission line, the currents flow in opposite directions, minimizing radiation. In contrast, along the two dipole arms, the currents flow in phase, leading to the efficient radiation of electromagnetic waves [33]. Considering the size of the test pipeline and the results of preliminary exploration, the resonant frequencies of the dipole antenna are initially set at 1.5 GHz and 2.5 GHz. This ensures that the antennas are of suitable dimensions for proper installation on the test pipeline to form an effective sensor, since the resonant frequencies affect antenna dimension. The use of two significantly different frequencies without mutual interference, combined with swept-frequency measurement, ensures reliable measurement performance. The resonant frequencies of the antenna are related to the lengths of the dipole arms. For the resonant frequencies of 1.5 GHz and 2.5 GHz, the corresponding free-space wavelengths are approximately 200 mm and 120 mm, respectively. Within the FR4 dielectric, these wavelengths are reduced to approximately 95 mm and 57 mm, respectively [34]. According to dipole antenna theory, the total length of a dipole arm is typically around 0.5 times the operating wavelength [35], which provides a theoretical basis for analyzing the arm lengths.

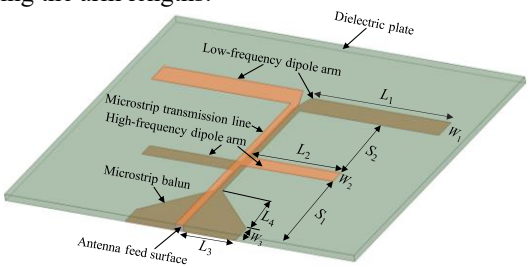

Fig. 2. Configuration of the dual-frequency printed dipole antenna.

In this study, we optimize the structural parameters L_1, L_2, L_3, L_4, S_1, S_2, W_1, W_2, and W_3, as shown in Fig. 2, using the finite element simulation method to achieve impedance matching and maintain low reflection coefficients for a dual-frequency dipole antenna. During the finite element simulation, the sweeping frequency ranges from 1 GHz to 3 GHz with a step size of 1 MHz. Radiation boundaries are set around the model, and the conductors are assigned perfect electric conductor boundaries. First, we analyze the influence of each parameter on the antenna performance and determine the optimization range for each parameter. Finally, we obtain the optimal parameters through comprehensive optimization. Fig. 3(a) and (b) show the influences of the length L_1 and the length L_2 on the reflection coefficient S_{11}. An increase in L_1 leads to a decrease in the low-frequency resonance frequency, while an increase in L_2 results in a lower high-frequency resonant frequency. This is consistent with dipole antenna theory [35], from which it follows that the resonance frequencies of a dipole antenna are inversely proportional to the lengths of its arms. We choose an initial value of L_1=36 mm and an initial value of L_2=23 mm to obtain resonant frequencies near 1.5 GHz and 2.5 GHz, respectively. The width of the dipole arm has a minor impact on both the resonant frequency and impedance. In this study, the

initial width of the low-frequency dipole arm W_1 is determined as 5.7 mm, and the initial width of the high-frequency dipole arm W_2 is determined as 3.7 mm.

The distance S_1 between the edges of the high-frequency dipole arm and the dielectric plate, and the distance S_2 between the edges of the low-frequency and high-frequency dipole arms, both influence the reflection coefficient S_{11}. Therefore, it is necessary to analyze the effects of different S_1 and S_2 values on antenna performance. The effects of varying S_1 and S_2 on the reflection coefficient S_{11} are presented in Fig. 4(a) and (b). The relationships between the reflection coefficient S_{11} and the variations in S_1 and S_2 are quite complex. To achieve resonance frequencies approximately at 1.5 GHz and 2.5 GHz, while achieving a lower reflection coefficient S_{11}, initial values of S_1 and S_2 are set as 26 mm and 22 mm, respectively.

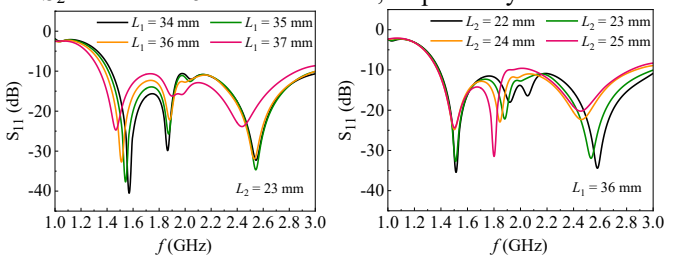

Fig. 3. (a) Effect of L_1 on reflection coefficient S_{11}. (b) Effect of L_2 on reflection coefficient S_{11}.

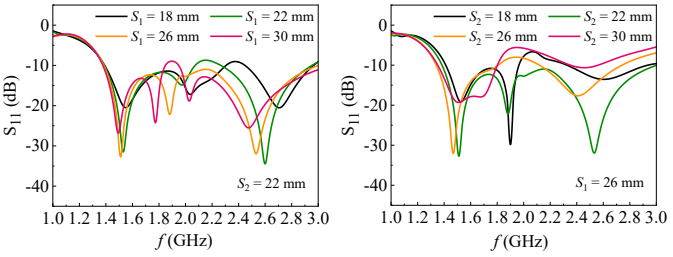

Fig. 4. (a) Effect of S_1 on reflection coefficient S_{11}. (b) Effect of S_2 on reflection coefficient S_{11}.

For achieving optimal impedance matching of the antenna, the determination of the parameters of the microstrip balun structure including the L_3 which is the half of the bottom edge length, the height of the tapered section L_4, and the width W_3 is very important. The influences of these parameters on the impedance including the real part Re and imaginary part Im are shown in Fig. 5. It is evident that each parameter exerts an influence on the impedance. To ensure the impedance is close to 50 Ω, initial values of L_3, L_4, and W_3 are set at 8 mm, 15 mm, and 4 mm, respectively.

In order to obtain an antenna configuration that meets the requirements, these parameters need to be comprehensively optimized. In this study, the optimization objectives for the antenna design are defined as achieving resonant frequencies of 1.5 GHz and 2.5 GHz, with S_{11} less than -40 dB and impedance close to 50 Ω at both frequencies. The optimized parameters and their variation ranges are shown in TABLE I. Min focus and max focus denote subranges of specified parameter values. During the optimization process, the search begins within these subranges to narrow the search space and quickly identify parameter values that meet the optimization objectives. If no satisfactory values are found, the search is expanded to the entire value range. The sequential nonlinear programming (SNLP) algorithm is used as the optimization method to determine the optimal design parameters for the antenna. The SNLP algorithm has the advantages that it exhibits faster convergence rates, effective constraint handling, and a significant reduction in noise. During the optimization process, the algorithm performs multiple optimization iterations, continuously updating the response surface model based on simulation results to systematically refine design parameters. This iterative process ultimately converges to the defined optimization objectives. When the objectives are met, the final optimized parameters are provided.

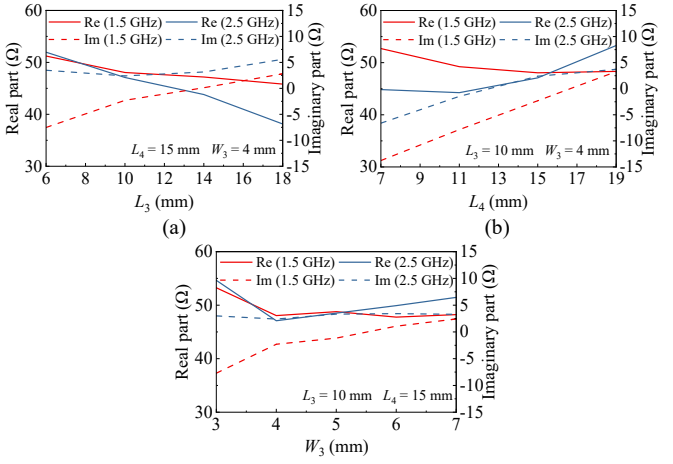

Fig. 5. (a) Effect of L_3 on impedance at 1.5 GHz and 2.5 GHz. (b) Effect of L_4 on impedance at 1.5 GHz and 2.5 GHz. (c) Effect of W_3 on impedance at 1.5 GHz and 2.5 GHz.

TABLE I
RANGE OF PARAMETER VALUES

Parameter	Value range (mm)	Min focus	Max focus
L_1	[23.75,50]	25	45
L_2	[14.25,30]	15	30
L_3	[8,18]	9	16
L_4	[6,16]	8	14
W_1	[3,6]	3	6
W_2	[3,6]	3	6
W_3	[3,7]	3	7
S_1	[18,30]	22	30
S_2	[18,30]	22	30

Based on the optimization results, the structural parameters of the printed dipole antenna were determined as follows: L_1=35.9 mm, L_2=23.7 mm, L_3=14.2 mm, L_4=12.7 mm, S_1=27 mm, S_2=23.4 mm, W_1=5.7 mm, W_2=3.7 mm, W_3=5.3 mm. Afterward, the printed dipole antenna was fabricated using printed circuit board (PCB) technology, and a vector network analyzer (VNA) was used for actual measurements of the reflection coefficient S_{11}. Fig. 6 shows the S_{11} values of the simulation results and the experimental results obtained from the VNA. During the transition from simulation to fabrication, fabrication tolerances and deviations were carefully considered, including PCB manufacturing inaccuracies, variations in substrate material properties, and assembly misalignments.

Nevertheless, differences between the experimental results and the simulation results were still observed. It can be attributed to factors such as inherent limitations in simulation accuracy, unavoidable differences in material properties between simulation and actual fabrication, and inevitable fabrication errors. These differences will not affect the ability of the sensor to measure solid concentration, as we utilize phase shifts of microwaves at two working frequencies and their relationships with solid concentration and moisture for measurement. We ultimately determine the actual working frequencies based on the experimental results, and the experimentally measured S_{11} values at these two frequencies are very low, ensuring good antenna performance and meeting the requirements for solid concentration measurement.

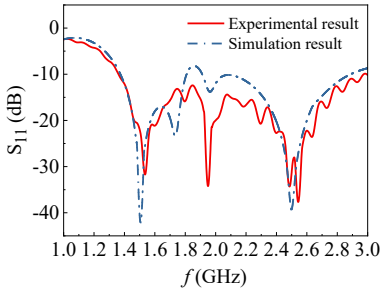

Fig. 6. S_{11} values of the simulation result and the experimental result.

C. Measurement system design

The main elements of the measurement system are shown in Fig. 7, which includes the VNA, coaxial cables, transmitting antenna, test pipeline and receiving antenna. The transmitting and receiving antennas are placed on opposite sides of the test pipeline to form a sensor that operates in the phase-based transmission modality. The port 1 of the VNA is used to generate microwave signals covering the frequency range from 1 GHz to 3 GHz, which are then conveyed to the transmitting antenna for emission through coaxial cables. Subsequently, the receiving antenna captures the microwave signal passing through the test pipeline, which is then conveyed to the port 2 of the VNA. The VNA can measure the phase shifts of microwaves at two working frequencies. The measured phase shifts at these frequencies provide information to simultaneously determine solid concentration and moisture content.

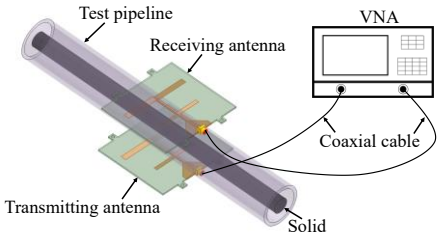

Fig. 7. Main elements of the measurement system.

III. EXPERIMENT TEST

Roping flow is a typical flow pattern in gas-solid two-phase flow. Given the feasibility of simulating roping flow pattern in the laboratory and the convenience of calculating its true solid concentration, roping flow is suitable for verifying the solid concentration measurement methods [25] [26]. The experimental setup is shown in Fig. 8, and the experiments were conducted in a laboratory environment, with the temperature and ambient humidity maintained at stable levels. The VNA has a frequency range of 1 MHz to 6.5 GHz with a frequency resolution of 1 Hz. Its measurement bandwidth has a range of 10 Hz to 50 kHz, and its dynamic range is 113 dB. The VNA can achieve sufficient resolution and accuracy in measuring phase shifts at the two working frequencies used in this study. The test pipeline is made of acrylic, which is generally considered a microwave-transparent material, to avoid causing significant impact on microwave propagation. The internal and external diameters (d_t and D_t) of the test pipeline are 35 mm and 42 mm, respectively. The PVC pipes fully filled with coal powder, as shown in Fig. 9(a), are used to simulate the solid phase of the roping flow. In Fig. 9(a), the internal diameters d_p of the PVC pipes from left to right are 13 mm, 15 mm, 18 mm, 20 mm, 23 mm, 26 mm, and 30 mm.

By inserting PVC pipes filled with coal powder with different diameters into the test pipeline, as shown in Fig. 9(b), a roping flow with varying solid concentrations is simulated [25]. By inserting the PVC pipes into the pipeline with different positions, roping flow with different phase distributions is simulated. All the PVC pipes have a length l of $12D_t$ to ensure that the simulated roping flow structure with the desired solid concentration is entirely within the sensing volume of the sensor. The true solid concentration S_c of roping flow is calculated from

$$S_c = \frac{V_p}{V_t} \times 100\% = \frac{\pi \left(d_p/2\right)^2 l}{\pi \left(d_t/2\right)^2 l} \times 100\% = \left(\frac{d_p}{d_t}\right)^2 \times 100\% \quad (5)$$

where V_p represents the volume of the solid, and V_t represents the volume of the test pipeline. In this study, for the PVC pipes filled with coal powder with different d_p, the calculated solid concentrations are 13.80%, 18.37%, 26.45%, 32.65%, 43.18%, 55.18%, and 73.47%.

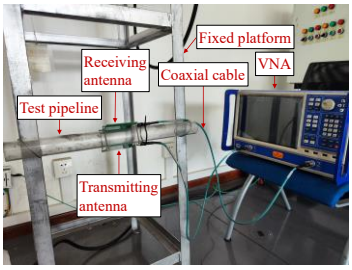

Fig. 8. Photograph of the experimental setup.

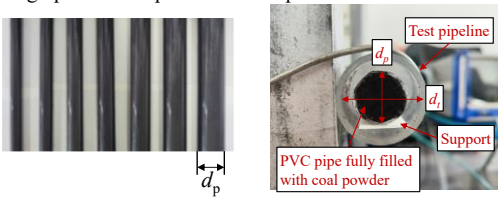

(a) (b)

Fig. 9. (a) PVC pipes fully filled with coal powder with different diameters. (b) Photograph of coal powder-filled PVC pipe insertion into the test pipeline.

To investigate the influence of moisture on the solid concentration measurement and to explore methods for

eliminating this influence, coal powder samples with varying moisture contents M_c are prepared. We use the weighing method to obtain water with a mass of m and dry coal powder with a mass of M. Then, the coal powder was spread out, water was sprayed evenly onto it, and it was thoroughly and uniformly mixed to make the water consistently distributed throughout the coal powder. In this way, coal powder with different moisture contents can be obtained, and its moisture content M_c is defined as:

$$M_c = \frac{m}{m+M} \times 100\% \tag{6}$$

In this study, coal powder with moisture contents of 0%, 2%, 4%, and 6% is prepared. Experiments were conducted under test conditions that cover all combinations of moisture contents (0%, 2%, 4%, and 6%) and solid concentrations (13.80%, 18.37%, 26.45%, 32.65%, 43.18%, 55.18%, and 73.47%).

IV. Results and Discussion

Based on the measured results of the reflection coefficient S_{11} shown in Fig. 6, the working frequencies of the sensor are determined as 1.534 GHz and 2.544 GHz. Fig. 10(a) and (b) present the phase shift θ measured at different frequencies for the PVC pipes fully filled with coal powder with different d_p under a moisture content M_c of 6%. Additionally, Fig. 11(a) and (b) show the measured phase shift θ at different frequencies with a constant d_p of 30 mm and different M_c. Fig. 10 shows that the phase shifts under both working frequencies are sensitive to the change of d_p when the M_c is fixed. Fig. 11 shows that the phase shifts under both working frequencies are sensitive to the change of moisture content M_c when the d_p is fixed. When microwaves propagate through a medium, the frequency, the propagation distance, and the medium permittivity all affect the phase characteristics of the microwaves. The value of the phase shift measured by the VNA decreases with increasing frequency, propagation distance, and medium permittivity. The increasing d_p increase the solid concentration and increase the mixture permittivity. The increasing moisture content also increases the mixture permittivity. Therefore, under the same condition of moisture content, an increase in solid concentration leads to a decrease in the value of the measured phase shift θ. Under the same condition of solid concentration, an increase in moisture content also leads to a decrease in the value of the measured phase shift θ. These results indicate that the phase shifts under both working frequencies can effectively acquire the information including the solid concentration and the moisture content.

To assess the performance of the sensor on measuring gas-solid flows with non-uniform phase distribution, we carry out phase shift measurement by placing a coal powder-filled PVC pipe at different positions in the test pipeline. In the horizontal direction, we select five measurement positions (1 to 5) at distances of 6.5 mm, 12 mm, 17.5 mm, 23 mm and 28.5 mm from the left inner wall of test pipeline. In the vertical direction, we select five measurement positions (6 to 10) at distances of 6.5 mm, 12 mm, 17.5 mm, 23 mm and 28.5 mm from the upper inner pipeline wall. We measured the distance from the center of the PVC pipe to the inner wall of the test pipeline, which allowed us to determine its position precisely. The PVC pipe was then fixed with support at the desired position. Fig. 12(a)-(d) shows the measured phase shifts at two resonant frequencies when a PVC pipe with d_p of 13 mm and M_c of 0% is placed at different positions in the test pipeline. We calculate the relative deviation (RD) of the measured phase shift at each position to the average phase shift of the five positions and the results are also shown in Fig. 12(a)-(d). The relative deviation can indicate the differences of the measured phase shifts at five positions which helps to evaluate the sensor output characteristics when the solid phase is at different positions. From Fig. 12(a)-(d) we can see that for each sweeping frequency range, although the PVC pipe is at different positions, the measured phase shifts under the same working frequency are close to each other. The relative deviations (RD) are all small especially when the sensor works at the high resonant frequency of 2.544 GHz. These results indicate that, at both low and high frequencies, the sensor exhibits relatively uniform sensitivity distributions, and the sensor outputs are not sensitive to solid distribution, thereby enabling it to measure solid concentrations under different solid distributions.

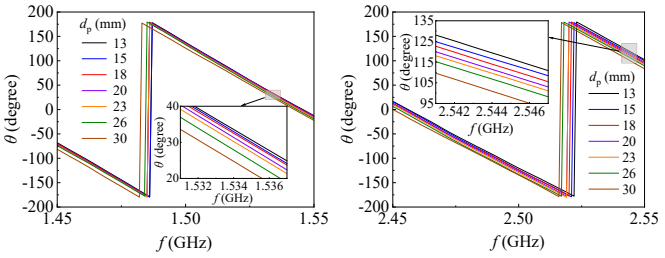

Fig. 10. Measured phase shifts at sweeping frequencies with varying d_p and a constant M_c of 6%: (a) 1.45–1.55 GHz; (b) 2.45–2.55 GHz. Increasing d_p leads to higher solid concentrations and results in decreased measured phase shifts.

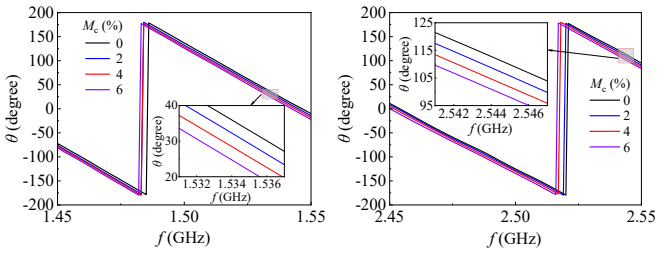

Fig. 11. Measured phase shifts at sweeping frequencies with varying M_c and a constant d_p of 30 mm: (a) 1.45–1.55 GHz; (b) 2.45–2.55 GHz. Increasing M_c leads to decreased measured phase shifts.

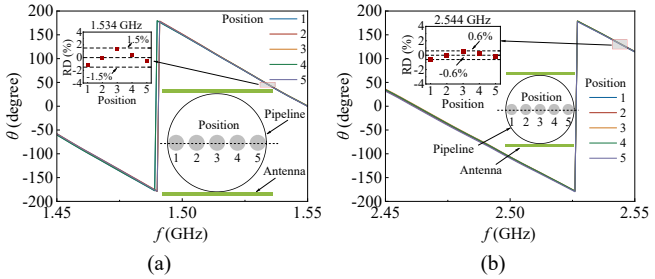

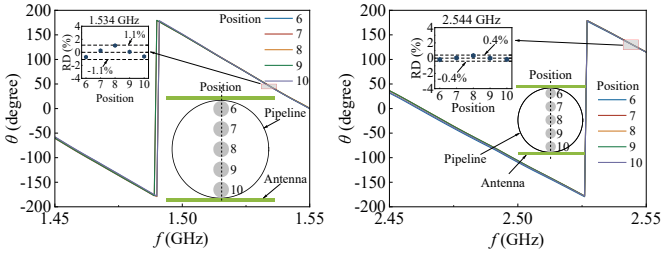

Fig. 12. Measured phase shifts at sweeping frequencies when the PVC pipe is placed at different positions: (a) 1.45–1.55 GHz, horizontal positions; (b) 2.45–2.55 GHz, horizontal positions; (c) 1.45–1.55 GHz, vertical positions; and (d) 2.45–2.55 GHz, vertical positions. The results show that the sensor exhibits a relatively uniform sensitivity distribution and is insensitive to the solid distribution.

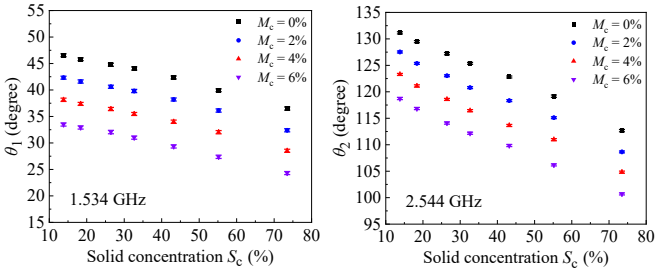

Fig. 13. Measured phase shifts with different solid concentrations under different moisture contents at (a) 1.534 GHz and (b) 2.544 GHz. The phase shifts decrease with increasing solid concentration at a fixed moisture content, and also decrease with increasing moisture content at a fixed solid concentration.

Based on the phase shift measurement results with different solid concentrations and moisture contents, we extract the phase shift values at two working frequencies of 1.534 GHz and 2.544 GHz, denoted as θ_1 and θ_2. Repeated experiments were conducted and phase shift values were obtained at both low and high resonant frequencies under various solid concentrations and moisture contents. The average phase shift values are calculated for each experimental condition, and error bars which represent the standard deviations of the measured phase shift are employed to reflect the measurement uncertainty. The measurement results at frequencies of 1.534 GHz and 2.544 GHz are shown in Fig. 13 (a) and (b). It can be seen in Fig. 13 (a) that when the moisture content is fixed, the measured phase shift θ_1 decreases with the increase of the solid concentration at 1.534 GHz. When the solid concentration is fixed, the measured phase shift θ_1 decreases with the increase of the moisture content at 1.534 GHz. Similarly, it can be seen in Fig. 13 (b) that when the moisture content is fixed, the measured phase shift θ_2 decreases with the increase of the solid concentration at 2.544 GHz. When the solid concentration is fixed, the measured phase shift θ_2 decreases with the increase of the moisture content at 2.544 GHz. Fig. 13 shows that the phase shifts at both working frequencies are sensitive to the solid concentration, but the phase shifts are affected by moisture. At high working frequency, the phase shifts are more sensitive to changes in the solid concentration. The error bars for both θ_1 and θ_2 are small, indicating high repeatability and low measurement uncertainty. Moreover, since the error bars for θ_2 are smaller, its measurement uncertainty is lower than that of θ_1. Fig. 13 indicates that only depending on phase shift information from a single resonant frequency is inadequate to accurately measure solid concentration when moisture content is an unknown variable. In order to eliminate the influence of moisture content on the measurement of solid concentration, a decoupling method is proposed. For the decoupling method as described before, it is important to establish the relationships among the phase shift, moisture content and solid concentration under two working frequencies. In this study, we establish these relationships based on the experimental data in Fig. 13. From the Fig. 13, it can be seen that when the moisture M_c is fixed, the solid concentration has a nearly linear relationship with the measured phase shift. The change of moisture content almost does not change the slope of the relationships but change the intercept of the relationships. We apply linear fitting to the data to establish the relationship between solid concentration and the measured phase shift under varying moisture conditions. Then a universal linear relationship can be built to describe the relationship between solid concentration and measured phase shift under varying moisture conditions. The slope S_1 of the relationship in Fig. 13(a) is determined as the mean value of the slopes when the M_c is 0%, 2%, 4% and 6% under the working frequency of 1.534 GHz. The slope S_2 of the relationship in Fig. 13(b) is determined as the mean value of the slopes when the M_c is 0%, 2%, 4% and 6% under the working frequency of 2.544 GHz. Based on the results of fitting method, the values of S_1 and S_2 are -16.10 and -29.88. respectively. The relationship between the intercept I_1 and the moisture M_c in Fig. 13(a) and the relationship between the intercept I_2 and the moisture M_c in Fig. 13(b) are determined by fitting method which are

$$I_1 = -220.35M_c + 49.22 \quad (7)$$

$$I_2 = -214.66M_c + 135.37 \quad (8)$$

The measured phase shift θ_1 and θ_2 are

$$\theta_1 = S_1 \times S_c + I_1 = -16.10 \times S_c - 220.35M_c + 49.22 \quad (9)$$

$$\theta_2 = S_2 \times S_c + I_2 = -29.88 \times S_c - 214.66M_c + 135.37 \quad (10)$$

Therefore

$$S_c = f_1(\theta_1, M_c) = \frac{-\theta_1 - 220.35M_c + 49.22}{16.10} \quad (11)$$

$$S_c = f_2(\theta_2, M_c) = \frac{-\theta_2 - 214.66M_c + 135.37}{29.88} \quad (12)$$

Then the new parameter Q is determined based on equations (4), (11) and (12).

The process described above is an experimental calibration of the sensor over the expected moisture range. It is a simple and effective approach to obtain the accurate relationships between the outputs of a new sensor system and the measured parameters, thereby ensuring its effectiveness in practical deployment. The moisture range was set from 0% to 6%, considering the moisture variations typically encountered during the pneumatic conveying of coal powder in blast furnaces. After building these relationships, experiments were carried out with different solid concentrations under different moisture contents to verify the effectiveness of the proposed method. In the process of decoupling method, for each selected moisture content which is the possible value of true moisture content, based on the measured θ_1 and θ_2 values, the solid

concentrations are calculated using equations (11) and (12). Then, the Q values corresponding to each selected moisture content are calculated. Since under each moisture content condition, we carry out experiments including many flow conditions with different solid concentrations, we calculate the average Q values of all flow conditions under a fixed moisture content and present the results in Fig. 14. The results of Fig. 14 demonstrate that the Q value reaches its minimum when the selected moisture content matches the true moisture content. Therefore, by calculating the Q values and finding the minimum Q value, the true moisture content is determined.

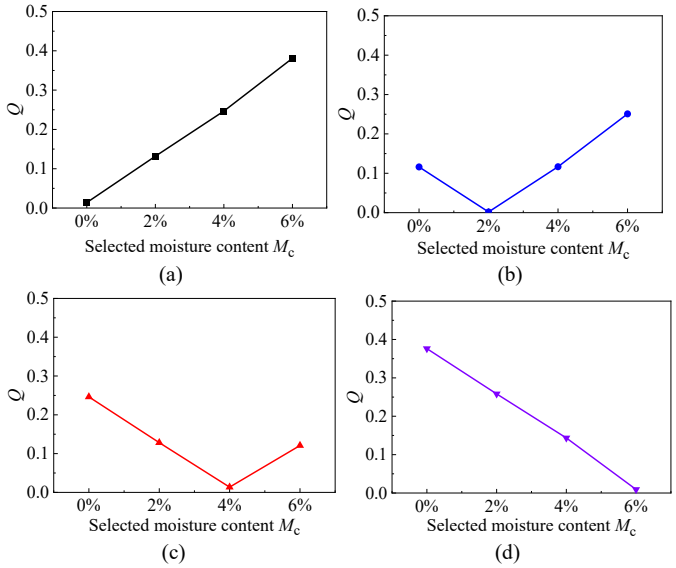

Fig. 14. (a) Q values with varying moisture content when the true moisture content is 0%. (b) Q values with varying moisture content when the true moisture content is 2%. (c) Q values with varying moisture content when the true moisture content is 4%. (d) Q values with varying moisture content when the true moisture content is 6%.

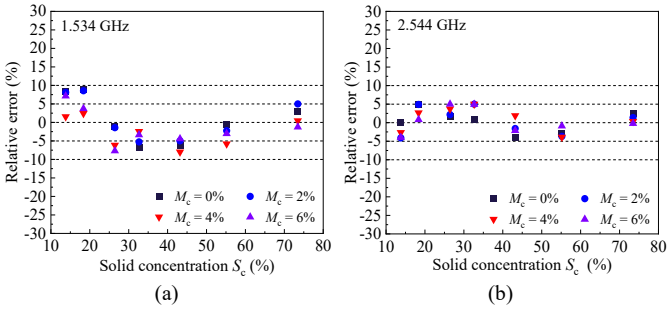

Fig. 15. Measurement errors of solid concentration at the working frequency of (a) 1.534 GHz. (b) 2.544 GHz.

Accurate determination of moisture content is essential for measuring solid concentration, since the measured θ_1 and θ_2 must be combined with the moisture content to obtain the solid concentration. Following the determination of solid concentrations, the measurement errors of solid concentration under different moisture content conditions at the working frequencies of 1.534 GHz and 2.544 GHz are shown in Fig. 15 (a) and (b), respectively. It can be seen that the measurement results are satisfactory. Especially at the high working frequency of 2.544 GHz, the relative errors are concentrated within ±5%, which is smaller than those at the low working frequency, where errors range from -9% to 9%. This can be attributed to higher sensitivity and lower measurement uncertainty at the high working frequency, which contribute to more accurate solid concentration measurements. The solid concentration measurement results demonstrate that the proposed method can determine the unknown moisture content and eliminate the influence of moisture on solid concentration measurement. Finally, a satisfactory measurement accuracy of the solid concentration is obtained under the conditions of unknown and varying moisture content.

V. Conclusion

This study has proposed a dual-frequency microwave transmission sensor, comprising printed dipole antennas, and a novel decoupling method to achieve moisture independent measurement of solid concentration. Conclusions resulting from the investigations are summarized as follows.

The dual-frequency phase shifts of the sensor are sensitive to both solid concentration and moisture content but are insensitive to the solid distribution. With a fixed moisture content, an increase in solid concentration results in a decrease in phase shift. For the same solid concentration, an increase in moisture content leads to a decrease in phase shift. Relying only on the measured phase shift at a single working frequency is inadequate to accurately measure solid concentration under the conditions of unknown and varying moisture content.

By employing the proposed dual-frequency microwave transmission sensor and decoupling method, both moisture content and solid concentration are extracted from the measured dual-frequency phase shifts. The solid concentration measured at the high working frequency exhibits a lower relative error compared to that at the low frequency, and for the tested range of solid concentrations between 13.80% and 73.47% and moisture contents from 0% to 6%, the relative error at the high frequency remains within ±5%. The proposed method exhibited good performance, being sensitive to solid concentration but insensitive to solid distribution. It showed good measurement reliability, and effectively eliminated the influence of moisture content, providing a novel approach for measuring solid concentration independently of moisture content. The proposed method can be generalized to other gas–solid systems with different solid materials, and one simple and effective approach is to perform an initial calibration of the sensor system using the target material to ensure accurate measurements, following the method described in this study. The application of the proposed method to different gas–solid systems with different solid distributions and parameter ranges will be considered in future research.

References

[1] Y. Yan, Y. Hu, L. Wang, X. Qian, W. Zhang, K. Reda, J. Wu, and G. Zheng, "Electrostatic sensors–Their principles and applications," Measurement, vol. 169, Feb. 2021, Art. no. 108506.

[2] C. Wang, L. X. Jia, and J. Ye, "Characterization of particle mass flow rate of gas–solid two-phase flow by the combination of transferred and induced current signals," IEEE Trans. Instrum. Meas., vol. 70, pp. 1–12, Jan. 2021.

[3] X. Qian, Y. Yan, S. Wu, and S. Zhang, "Measurement of velocity and concentration profiles of pneumatically conveyed particles in a

square-shaped pipe using electrostatic sensor arrays," Powder Technol., vol. 377, pp. 693–708, Jan. 2021.
[4] W. Zhang, C. Wang, W. Yang, and C.-H. Wang, "Application of electrical capacitance tomography in particulate process measurement – A review," Adv. Powder Technol., vol. 25, no. 1, pp. 174–188, Jan. 2014.
[5] X. X. Wang, Y. Hu, H. Hu, and L. Li, "Evaluation of the performance of capacitance sensor for concentration measurement of gas/solid particles flow by coupled fields," IEEE Sens. J., vol. 17, no. 12, pp. 3754–3764, Jun. 2017.
[6] Q. Guo, M. Ye, W. Yang, and Z. Liu, "A machine learning approach for electrical capacitance tomography measurement of gas–solid fluidized beds," AIChE J., vol. 65, no. 6, Jun. 2019, Art. no. e16583.
[7] Y. Han and C. Tan, "Measurement of particle concentration by multifrequency ultrasound attenuation in liquid–solid dispersion," IEEE Trans. Ultrason. Ferroelectr. Freq. Control, vol. 68, no. 3, pp. 843–853, Mar. 2021.
[8] J. M. Furlan, V. Mundla, J. R. Kadambi, N. C. Hoyt, R. J. Visintainer, and G. Addie, "Development of A-scan ultrasound technique for measuring local particle concentration in slurry flows," Powder Technol., vol. 215–216, pp. 174–184, Jan. 2012.
[9] J. Fan, F. Wang, H. Cui, and W. Wang, "Concentration determination in a cylinder-simulated gas–solid two phase flow using ultrasonic backscattering method," Appl. Acoust., vol. 203, Feb. 2023, Art. no. 109212.
[10] I. R. Barratt, Y. Yan, and B. Byrne, "A parallel-beam radiometric instrumentation system for the mass flow measurement of pneumatically conveyed solids," Meas. Sci. Technol., vol. 12, no. 9, pp. 1515–1528, Aug. 2001.
[11] R. B. Spelay, S. A. Hashemi, R. S. Sanders, and B. T. Hjertaker, "Improved scatter correction model for high attenuation gamma-ray tomography measurements," Meas. Sci. Technol., vol. 32, no. 8, May 2021, Art. no. 085903.
[12] Z. Guo and G. Zhang, "Application of a microwave mass flow meter in a dense phase pneumatic conveying system of pulverized coal," 2018 IEEE 3rd Advanced Information Technology, Electronic and Automation Control Conference (IAEAC), Chongqing, 2018, pp. 2547-2551.
[13] L. Pang, Y. Shao, C. Geng, W. Zhong, G. Liu, L. Liu, and W. Tian, "Measurement of solid mass flow rate by a non-intrusive microwave method," Powder Technol., vol. 323, pp. 525–532, Jan. 2018.
[14] Z. Akhter, W. Taha, M. S. U. Rahman, and M. A. Abou-Khousa, "Detection of solid contaminants in gas flows using microwave resonant probes," Meas. Sci. Technol., vol. 32, no. 3, Dec. 2020, Art. no. 035109.
[15] J. Zou, C. Liu, H. Wang, and Z. Wu, "Mass flow rate measurement of bulk solids based on microwave tomography and microwave Doppler methods," Powder Technol., vol. 360, pp. 112–119, Jan. 2020.
[16] C. S. Oon, M. Ateeq, A. Shaw, A. Al-Shamma'a, S. N. Kazi, and A. Badarudin, "Experimental study on a feasibility of using electromagnetic wave cylindrical cavity sensor to monitor the percentage of water fraction in a two phase system," Sens. Actuator A-Phys., vol. 245, pp. 140–149, Jul. 2016.
[17] P. Sharma, L. Lao, and G. Falcone, "A microwave cavity resonator sensor for water-in-oil measurements," Sens. Actuator B-Chem., vol. 262, pp. 200–210, Jun. 2018.
[18] W. Liu, N. Jin, D. Wang, Y. Han, and J. Ma, "A parallel-wire microwave resonant sensor for measurement of water holdup in high water-cut oil-in-water flows," Flow Meas. Instrum., vol. 74, Aug. 2020, Art. no. 101760.
[19] Y. Yang, Y. Xu, C. Yuan, J. Wang, H. Wu, and T. Zhang, "Water cut measurement of oil–water two-phase flow in the resonant cavity sensor based on analytical field solution method," Measurement, vol. 174, Apr. 2021, Art. no. 109078.
[20] M. A. Karimi, M. Arsalan, and A. Shamim, "Extended throat venturi based flow meter for optimization of oil production process," IEEE Sens. J., vol. 21, no. 16, pp. 17808–17816, Aug. 2021.
[21] C. Zhao, G. Wu, and Y. Li, "Measurement of water content of oil-water two-phase flows using dual-frequency microwave method in combination with deep neural network," Measurement, vol. 131, pp. 92–99, Jan. 2019.
[22] Y. Tu, L. Qin, E. Li, H. Ma, Y. Zhang, Y. Gao, C. Gao, J. Long, G. Guo, Y. Qiu, J. Li, H. Wu, and X. Zhao, "Application of time-domain gating technique in water content measurement of gas–liquid two-phase flow," Rev. Sci. Instrum., vol. 92, no. 9, Sep. 2021, Art. no. 094702.
[23] Q. Zeng, Q. Liu, G. Li, and H. Jiang, "A horn antenna with circular aperture for pipeline water cut measurement," Microw. Opt. Technol. Lett., vol. 64, no. 5, pp. 933–938, Feb. 2022.
[24] A. Penirschke, A. Angelovski and R. Jakoby, "Moisture insensitive microwave mass flow detector for particulate solids," 2010 IEEE Instrumentation & Measurement Technology Conference Proceedings, Austin, TX, USA, 2010, pp. 1309-1313.
[25] D. Wang, J. Sun, Y. Wang, G. Yang, Z. Zhu, and Z. Xie, "Eliminating the influence of moisture on solid concentration measurement in gas-solid flows using combined sensors," IEEE Trans. Instrum. Meas., vol. 72, pp. 1–10, 2023, Art no. 7500310.
[26] D. Wang, X. Liu, Y. Wang, Z. Zhu, D. Chen and Z. Xie, "Measurement of solid concentration in gas–solid flows using a microwave resonant cavity sensor," IEEE Trans. Instrum. Meas., vol. 73, pp. 1-9, 2024, Art no. 7501009.
[27] D. Wang, N. Jin, J. Ma, and Y. Ren, "Measurement of water holdup in oil–gas–water slug flow using microstrip antenna," IEEE Trans. Instrum. Meas., vol. 70, pp. 1–10, Jan. 2021, Art no. 8004310.
[28] J. Ma, N. Jin, D. Wang, D. Liu, and W. Liu, "Measurement of water holdup in vertical upward high water-cut oil-in-water flows using a high frequency sensor," Sens. Actuator A-Phys., vol. 289, pp. 165–179, Apr. 2019.
[29] Q. He, B. Wang, and J. He, "Wideband and dual-band design of a printed dipole antenna," IEEE Antennas Wirel. Propag. Lett., vol. 7, pp. 1–4, 2008.
[30] Z. Liang, Y. Li, X. Feng, J. Liu, J. Qin, and Y. Long, "Microstrip magnetic monopole and dipole antennas with high directivity and a horizontally polarized omnidirectional pattern," IEEE Trans. Antennas Propag., vol. 66, no. 3, pp. 1143–1152, Mar. 2018.
[31] E. L. Holzman, "Wideband measurement of the dielectric constant of an FR4 substrate using a parallel-coupled microstrip resonator," IEEE Trans. Microw. Theory Tech., vol. 54, no. 7, pp. 3127–3130, Jul. 2006.
[32] Y. Gou, S. Yang, J. Li, and Z. Nie, "A compact dual-polarized printed dipole antenna with high isolation for wideband base station applications," IEEE Trans. Antennas Propag., vol. 62, no. 8, pp. 4392–4395, Aug. 2014.
[33] C. A. Balanis, "Antenna theory: a review," Proc. IEEE, vol. 80, no. 1, pp. 7–23, 1992.
[34] L.-C. Kuo, H.-R. Chuang, Y.-C. Kan, T.-C. Huang, and C.-H. Ko, "A study of planar printed dipole antennas for wireless communication applications," J. Electromagn. Waves Appl., vol. 21, no. 5, pp. 637–652, Jan. 2007.
[35] K. Xiang, F. Chen, Q. Tan, and Q. Chu, "Design of novel printed filtering dipole antennas," IEEE Trans. Antennas Propag., vol. 69, no. 5, pp. 2537–2545, May 2021.